Full Length Research Paper

Determination of temperature effect on mechanical properties of templated mesoporous silica aerogels by nanoindentation method

Yilmaz Kucuk

Department of Mechanical Engineering, Bartin University, 74100 Bartin-Turkey E-mail: yilmazkucuk75@gmail.com. Tel: +90 378 223 5410. Fax: +90 378 223 5258.

Cross-linking is known as a chemical process to improve the mechanical properties by adding polymer. Therefore, the pore walls of aerogels can be strengthened by coating with polymer. In this study, the mechanical properties of a cross-linked monolithic silica aerogel have been examined by nanoindentation tests at different temperatures. Creep compliance values were analyzed as a function of time by linear viscoelastic equations using the test data of nanoindentation. It is determined that the creep compliance values obtained from nanoindentation are much higher than that of compressive test. Additionally, from the relaxation modulus curves, it can be expressed that the aerogel sample used retains its general long-term viscoelastic behavior at elevated temperatures.

Key words: Silica aerogel, nanoindentation, creep behavior, temperature test, linear viscoelasticity, depth-sensing indentation.

INTRODUCTION

Silica aerogel is an open-pored transparent material with optical and thermal properties that makes the material very interesting as an insulation material in windows and building (Fricke, 1992; Duer and Svendsen, 1998). Aerogel is a weak material in terms of tensile stress and moisture resistance. Therefore, these materials have to be protected against the harmful effects of environment. Conversely, they have a compression-resistant structure that could be used in some sandwich structures. Silica aerogel within a monolithic form requires gentle handling because of their fragile structure that emerging as a result of their low density as well as their high porosity structures (Lucas et al., 2004; Woignier et al., 1992). In some studies, it was focused on changing of the pore size and morphologies to improve the mechanical properties of aerogels (Kruk et al., 1997; Huo et al., 1996; Vartuli et al., 1994; Zhuravlev, 1993; Ogura et al., 2004). Recently, Leventis et al., (2008) produced some silica-based aerogels via a method where the native –OH

surface functionality of typical base-catalyzed sol–gel silica is employed as a template that directs conformal polymerization of isocyanates on the mesoporous surfaces. Depth-sensing indentation (DSI) (Fischer, 2002) which is also often called as nanoindentation, determines the mechanical properties such as hardness and elastic modulus, yield stress as well as parameters of strain hardening, creep or viscoelastic response, and even some fracture mechanics parameters (Mencik, 2005). In this method, indenter load and penetration depth are measured continuously during loading and unloading that could be controlled as low as several mN. This sensitivity is also valid for corresponding depths of penetration in the size of nanometer.

Temperature is a main agent affecting the mechanical properties of materials. It is known that the thermal conductivity of an aerogel is very low, around 15–20 mW m^{-1} K^{-1} under atmospheric pressure (Duer and Svendsen, 1998). Thermal fluctuations continuously affect the shape of polymers in liquid solutions since the temperature strongly affects the physical behaviour of polymers in a solution. To improve the mechanical properties of the aerogel sample, the polymer nano-encapsulation process can be implemented to the porous

structure of a silica-based aerogel (Leventis et al.2008),In literature, the nanoindentation tests are generally carried out at ambient temperatures. In other words, it has been detected that the studies regarding the use of high-temperature nanoindentation are not enough. Schuh et al. (2006) studied on high temperature nanoindentation to determine the thermal stability of the indentation equipment by using the fused silica. Beake and Smith (2002) have reported high temperature nano-indentation experiments on fused silica and soda–lime glass. Volinsky et al. (2004) and Sawant and Tin (2008) have recently reported the uses of high temperature nano-indentation for characterizing the mechanical properties of hard thin films and single crystal super-alloys. Lu et al. (2009), have recently used the high temperature nanoindenter to measure the mechanical properties of polymer resins at elevated temperatures. In another study, Fulcher et al. (2010) used the high-temperature indentation technique to examine the thermomechanical and shape-recovery behavior of a thermosetting, epoxy-based shape memory polymer (SMP).

It is clear that there is a need to do a new study for understanding of mechanical behaviors of cross-linked mesoporous silica aerogels at elevated temperatures. For this purpose, some nanoindentation tests at different temperatures as well as the room temperature were carried out by using hot-stage nanoindentation technique to determine the effect of temperature on the mechanical properties of a mesoporous silica monolith.

THEORY

In this study, it was assumed that the aerogel sample used has the linear viscoelastic properties and so it was provided formulas used for extracting the linear viscoelastic properties from nanoindentation data as a function of time. Lu et.al (2006), denoted in their study that the Berkovich indenter is modeled as a rigid conical indenter. For the indentation problem in which a rigid conical indenter is indenting into an elastic half-space, Sneddon (1965) derived relationship between load and displacement,

$$h^2 = \frac{\pi(1-v)\tan\alpha}{4G}P \tag{1}$$

where P and h are load and displacement, respectively, α the angle between the cone generator and the substrate plane, v the Poisson's ratio, and G the shear modulus.

Lee and Radok (1960) proposed an integral operator to determine the time-dependent stresses and deformations. Applying this technique to Equation (1) leads to the following time-dependent indentation depth under a prescribed arbitrary indentation loading history $P(t)$ in a linear viscoelastic material (Lu et al., 2006),

$$h^2(t) = \frac{\pi(1+v)\tan\alpha}{4}\int_0^t J(t-\xi)\left[\frac{dP\xi}{d\xi}\right]d\xi \tag{2}$$

where $J(t)$ is the creep compliance in shear at time t. Under a ramp loading, $P(t)=v_0 t$, differentiation of Equation (2) leads to (Lu et al.,2006),

$$J(t) = \frac{8h}{\pi(1-v)v_0\tan\alpha}\frac{dh(t)}{dt} \tag{3}$$

where v_0 is the loading rate. Equation (3) provides a direct differentiation method to determine the creep compliance in shear.

In another method to determine the creep compliance of a linear viscoelastic material can be expressed by the generalized Kelvin model (Lu et al., 2006),

$$J(t) = J_0 + \sum_{i=1}^{N} J_i\left(1 - e^{-t/\tau_i}\right) \tag{4}$$

where J_0, J_i are compliance numbers, and τ_i is retardation time.

Under $P(t)=v_0 t$, substituting Equation (4) into (2) leads to (Lu et al.,2006),

$$h^2(t) = \frac{1}{4}\pi(1+v)\tan\alpha\left[\left(J_0 + \sum_{i=1}^{N} J_i\right)\right.$$
$$\left.\right)P(t) - \sum_{i=1}^{N} J_i(v_0\tau_i)\left(1 - e^{-\frac{P(t)}{v_0\tau_i}}\right)\right] \tag{5}$$

After fitting Equation (5) to the load–displacement curve from nanoindentation, all parameters, J_0, J_i ($i =1, . . ., N$) and τ_i can be obtained. The creep compliance can be subsequently determined using Equation (4). Once $J(t)$ is obtained, other viscoelastic functions, such as the uniaxial relaxation modulus $E(t)$, can be determined. For example, the creep function in shear, $J(t)$, can be converted to $E(t)$ through the following relation under condition of a constant Poisson's ratio, v (Lu et al., 2006).

$$\int_0^t E(\tau)J(1-\tau)d\tau = 2(1+v)t \tag{6}$$

MATERIAL AND EQUIPMENT

Leventis et al. (2008) prepared some polymer nano- encapsulated silica monoliths, which have different chemical compositions,

Table 1. Chemical composition of the sample.

Sample ID	.0 M HNO_3 (g)	Pluronic P123[a] (g)	TMB (g)	TMOS (g)	N3200/acetone (g/mL)
X-MP4-T045	12	4	0.45	5.15	11/94

[a] Pluronic P123 (tri-block co-polymer: $PEO_{20}PPO_{70}PEO_{20}$)

Figure 1. Nano Indenter G200.

Table 2. Nano Indenter G200 Specifications.

Specification	Value
Displacement resolution	<0.01 nm
Maximum indentation depth	>500 μm
Maximum load (Standard)	500 mN
Maximum load with DCM option	10 mN
Maximum load with high-load option	10 N
Load resolution	50 nN
Contact force	<1.0 μN

and they labeled the samples in accordance with the Nakanishi's notation (Amanati et al., 2005). One of the samples produced by Leventis et al. (2008) was used in this study, which is coded as X-MP4-T045 11/94, for the hot-stage nanoindentation test.

This sample was prepared in a cylindrical form that having 10 mm in diameter and 3 mm in thickness and its flat surfaces were polished. The chemical composition of the sample is given in Table 1. In addition to the room temperature (RT), three different temperatures (50, 75, and 90ºC) were selected as testing temperatures. Higher temperatures than 90ºC were used for nanoindentation tests but a meaningful consistency between the response data could not be obtained. This situation can be explained with the pyrolysis occurred in the structure of polymer

during the test. A nanoindentation device which is called 'Nano Indenter® G200' by Agilent Technologies and its hot-stage indentation module were used for the indentation tests. By means of the heater and cooler systems of this device, the test temperatures could be controlled in the range of ±2ºC for each temperature. The Nano Indenter® G200 system is integrated with software, which is called as 'NanoSuite'. Additionally, a software package called as 'ANALYST' that allows the graphically comparing ofmultiple samples, is also available in the system. The Nano Indenter® G200 system is shown in Figure 1 and its specifications are given in Table 2. In this study, Berkovich (TB15294 ISO) indenter tip, which has the tip angle of 130.6º, was used.

For indentation processes, many tests have been carried out to ensure the consistency of result data in terms of loading-unloading curves. Also, the distance between indents for both X and Y directions was selected as 100 μm and the indentation tests were carried out in a matrices form of 10 by 10 indents at the (RT). The test parameters are given in Table 3.

The heater block of system used is shown in Figure 2. The sample is fixed on this tray and so, heating and cooling units of the system can control the temperature of sample.

RESULTS AND DISCUSSION

In RT, many indentation tests were carried out to determine the consistency of data. In Figure 3, it can be seen that the sample exhibits consistent data with regard to the curves of load-displacement and this situation is confirmed by the data that showed in Table 4. In other words, the aerogel sample introduces significant discrepancies depending on the changing of hardness and elastic modulus. As is known, the aerogels have very low thermal conductivity and by means of this characteristic, the effects of temperature fluctuations can be interpreted more clearly. Since the crosslinking process is carried out by adding polymer, some points of indent may have more polymers in their location, especially in a wall of pore and so, the variations in hardness values may cause to inconsistencies in the depths of nanoindentation by increasing temperature. All curves that represent the mean values are shown in Figure 3 as a black thick curve for each temperature test.

In order to determine the maximum depths and recovery capability of cross-linked aerogel sample, all of curves at each temperature are shown in Figure 4. As seen in Figure 4, both of the indentation depth and drift ratios increase with increasing temperatures. This situation can be explained by the effect of polymer. At room temperature, the maximum depth (h_{max-RT}) value was measured from loading step as 3134 nm and, the drift ($h_{drift-RT}$) value was 2411 nm at the end of unloading step. According to RT values, the $h_{max-50 ℃}$ and the h_{drift-}

Table 3. Test parameters.

Indenter Tip	Max. load	Holding time at peak load	Loading rate
Berkovich(TB15294 ISO)	10 mN	10 s	0.1 mN/s

Figure 2. Heater block.

$_{50°C}$ values increase by 6.34 and 9.12%, respectively. Similarly, for 75 and 90°C temperatures, these increasing ratios were calculated as 11.64 and 13.78% for indentation depth values. Increasing values of drift were determined as 14.72 and 28.41%, respectively. From these calculations, it can be denoted that the aerogel sample has a capability of recovery at the end of the unloading step and this ability is increased with increasing temperatures.

Table 4 shows a summary of the test results of nanoindentation obtained from different temperatures. In addition to the result data of nanoindentation test, a result of Young's modulus that obtained from a compressive test that performed by Leventis et al. (2008) is also showed in Table 4. It is clearly seen that the results of indentation test are higher about 6.6 times than that of compressive test. The difference between the results of mechanical test and the output data of software that used with a nano device were also reported in some similar studies that used comparative analysis (Lu et al., 2006; Sadr et al., 2009). It can be seen from Table 4 that the values of standard deviation increase with increasing temperatures while the values of Young's modulus and Hardness decrease about 50.8 and 6.38%, respectively when the temperature comes to 50°C. The decreasing ratios do not have a linear trend in increasing temperatures. Eventually, when the temperature reaches up to 75 and 90°C these ratios were calculated as about

-59.2, -21.27 and -66.42, -29.78%, respectively. In these calculations, the values of RT were taken into account as a base point. Nevertheless, the maximum depth of indentation does not attain to extreme values, so the increasing ratio in maximum depth is only +13.14% at 90°C.

The experimental load–displacement data used in Equation (5), and so, the fitted curves are plotted in Figure 5. It is seen that Equation (5) can describe the nanoindentation data very well. In the computation, the Poisson's ratio of aerogel sample was selected as 0.35.

The creep compliance curves that in average values for each temperature are given in Figure 6. The actual loading rate was calculated from the loading history observed from the output results, and used in analysis to determine the viscoelastic functions. By means of the loading data, the creep compliance values $J(t)$ and retardation times τ were calculated by using Equation (5) and Equation (4), respectively. As expected, the $J(t)$ values increase with increasing temperature. At elevated temperatures, when the time reachs up to 10^4 s, the $J(t)$ values are very close to each other, especially at. The values of $J(t)$ that obtained from 75 and 90°C are higher about 1.5 times than that of RT. Another attractive point in Figure 6 is that the $J(t)$ values that obtained from RT, 50 and 90°C have almost the same values between the time range of 10^2 and 10^3 s. After this time when the time of 10^3 s is exceeded, these points of convergence turn into the divergence and so the difference among creep curves increase depending on the time.

The average Young's relaxation modulus over time, is calculated from inversion of the average value of creep compliance for each temperature. The average creep compliance, in turn, has been calculated by averaging the creep coefficients corresponding to the same retardation times. After the creep calculations, the relaxation moduli of the sample can be calculated as a function of time.The relaxation modulus curves are shown in Figure 7. In Figure 7, the relaxation curves are seen close to each other except for the curve of RT. It can be clearly seen that all the relaxation curves that in the range between 9×10^3 s and 10^4 s are close to straight and are parallel to each other. The difference ratio between RT and 50°C is -25.42% and the difference ratio increases to -35.59% at 90°C.

Conclusions

In this study, some nanoindentation tests have been carried out to determine mechanical and viscoelastic
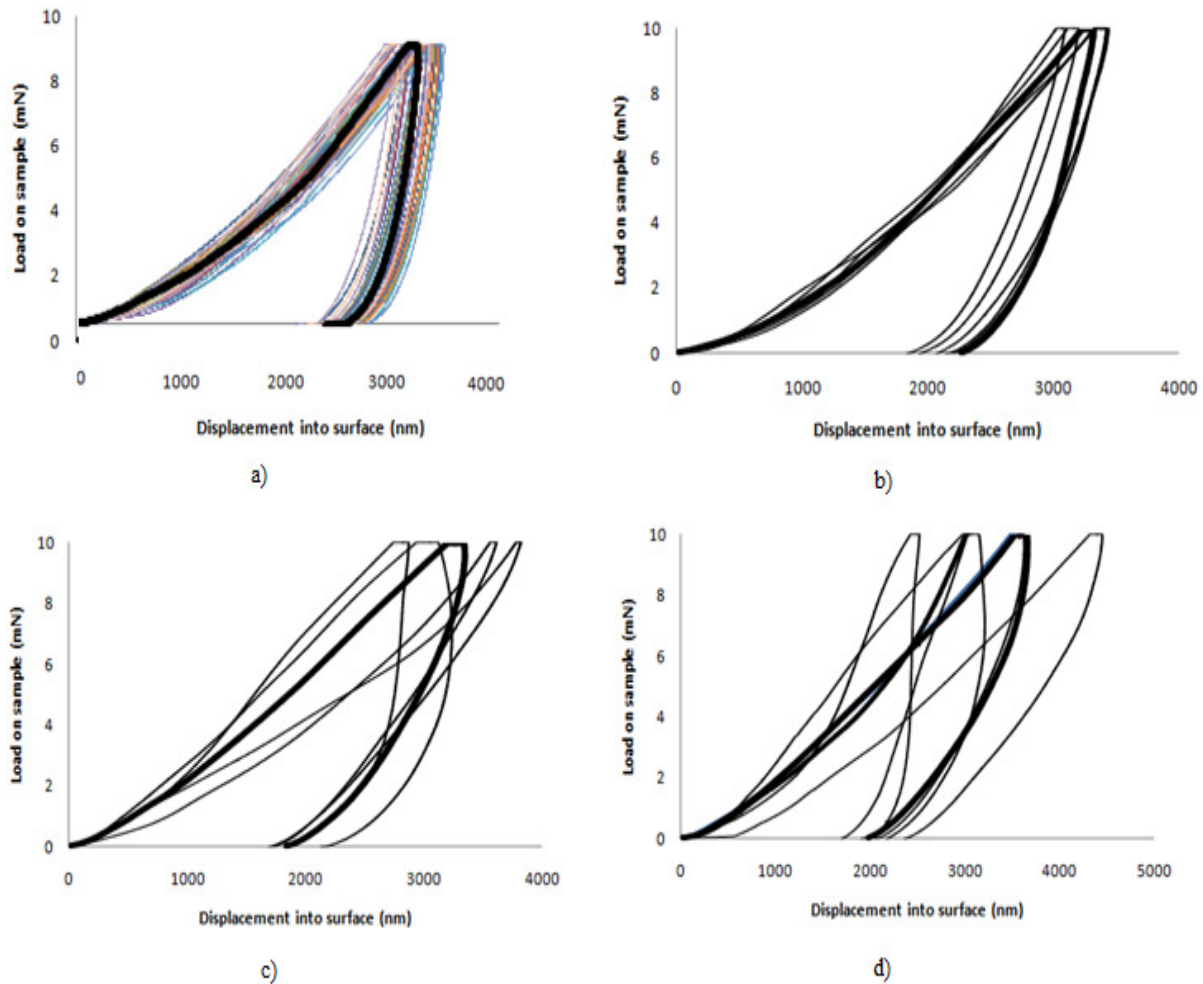
Figure 3. Mean Load vs. Displacement curves of nanoindentation tests at each temperature. Thicker curves show the mean curve. The discrepancies among the curves become more obvious with increasing temperature a) RT, b) 50°C, c) 75°C, and d) 90°C.

Table 4. Summary results of compressive and nanoindentation tests.

Temperature (°C)	E^a (MPa)	E^b (MPa)	H^b (MPa)	Mean indentation depth (nm)
RT	274±39	1826±266	47±8	3134±181
50°C	-	897±167	44±12	3333±265
75°C	-	745±234	37±14	3499±429
90°C	-	613±309	33±15	3566±497

[a]Young's modulus from compressive test; [b]Nanoindentation test.

properties of silica based aerogel sample at elevated temperatures. It can be said that the linear viscoelastic model can be used to examine the test results to calculate the creep compliance and relaxation modulus of the aerogel sample used in this study. By means of cross-linking process, the silica aerogel sample that comprise polymer in its mesoporous structure exhibits

significant discrepancies with regard to load-displacement values at elevated temperatures. With increasing temperature, the relaxation modulus of aerogel sample reaches to steady state. Additionally, the creep compliance values of the sample that obtained from the nanoindentation test were much higher that about 6.6 times than that of compressive test.
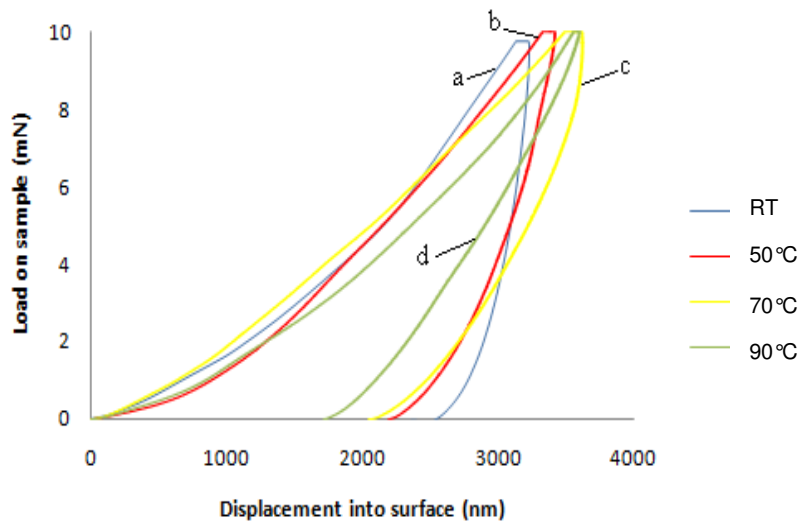
Figure 4. Load vs. Displacement curves of aerogel sample at elevated temperatures a) RT, b) 50°C, c) 75°C, d) 90°C.
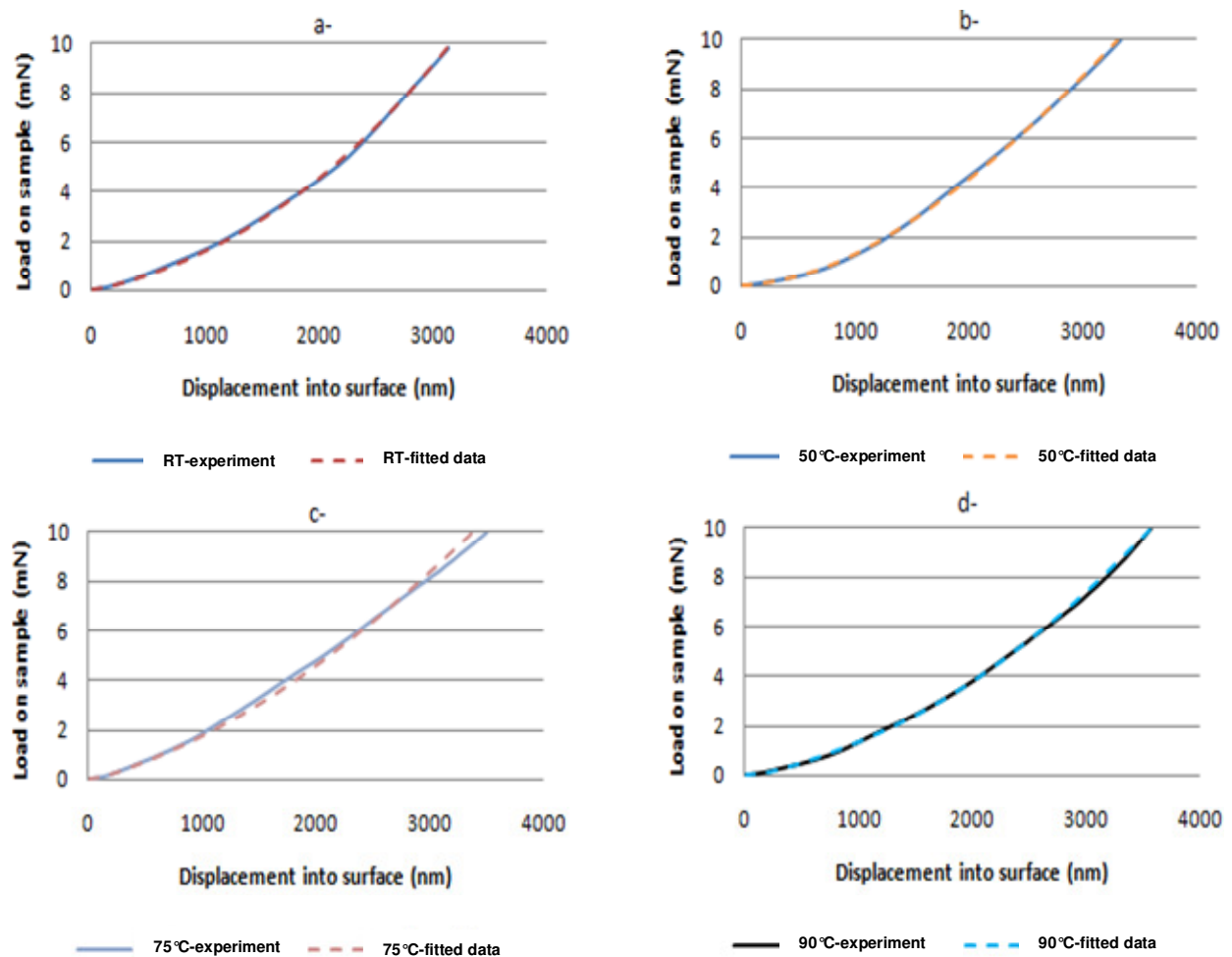
Figure 5. Load vs. displacement data for the loading segment in a typical indentation for each temperature. The continuous lines represent raw data from the nanoindentation experiment and the dashed lines show result of curve fitting. Good fitting was achieved for all materials in the selected loading range ($R > 0.9999$). a) RT, b) 50°C, c) 75°C, d) 90°C.
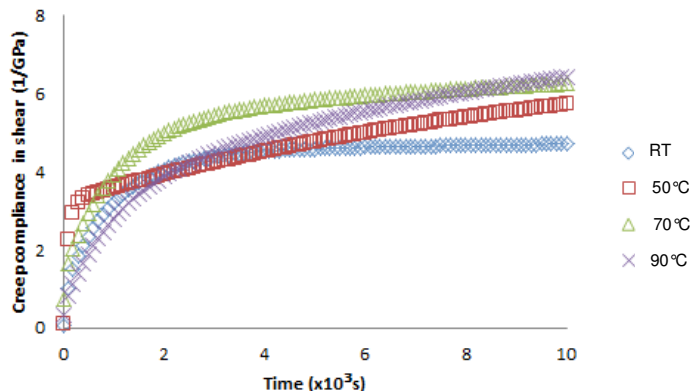
Figure 6. Creep compliance vs. Time curves obtained from the nanoindentation test for each temperature.
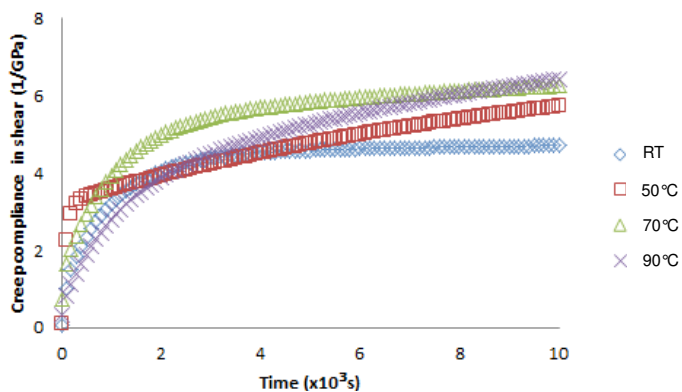
Figure 7. Relaxation modulus vs. Time curves obtained from the nanoindentation test for each temperature.

REFERENCES

Duer K, Svendsen S (1998). Monolithic silica aerogel in superinsulating glazings. Solar Energy, 63(4):259.

Fricke J (1992). Aerogels and their applications. J. Non-Cryst. Solids, 147: 148-356.

Lucas EM, Doescher MS, Ebenstein DM, Wahl KJ, Rolison DR (2004). Silica aerogels with enhanced durability, 30-nm mean pore-size, and improved immersibility in liquids. J. Non-Cryst. Solids, 350: 244.

Woignier T, Phalippou J, Hdach H, Larnac G, Pernot F, Scherer GW (1992). Evolution of mechanical properties during the alcogel-aerogel-glass process. J. Non-Cryst. Solids, 672: 147–148.

Kruk M, Jaroniec M, Sayari A (1997). Adsorption study of surface and structural properties of mcm-41 materials of different pore sizes. J. Phys. Chem. B., 101(4): 583.

Huo QS, Margolese DI, Stucky GD (1996). Surfactant control of phases in the synthesis of mesoporous silica-based materials. Chem. Mater., 8(5): 1147.

Vartuli JC, Schmitt KD, Kresge CT, Roth WJ, Leonowicz WME, McCullen SB, Hellring SD, Beck JS, Schlenker JL, Olson DH, Sheppard EW (1994). Effect of surfactant/silica molar ratios on the formation of mesoporous molecular sieves: inorganic mimicry of surfactant liquid-crystal phases and mechanistic implications. Chem. Mater., 6(12): 2317.

Zhuravlev LT (1993). Surface characterization of amorphous silica-a review of work from the former USSR. Colloid Surf. A – Physicochem. Eng. Aspects, 74(1): 71.

Ogura M, Miyoshi H, Naik SP, Okubo T (2004). Investigation on the drying induced phase transformation of mesoporous silica; a comprehensive understanding toward mesophase determination. J. Am. Chem. Soc., 126(35): 10937.

Leventis N, Mulik S, Wang X, Dass A, Patil VU, Leventis CS, Lu H, Churu G, Capecelatro A (2008). Polymer nano-encapsulation of templated mesoporous silica monoliths with improved mechanical properties. J. Non-Cryst. Solids., 354(2-9): 632.

Fischer-Cripps AC (2002).Nanoindentation. 2nd ed. New York: Springer.USA

Mencik J (2005). 22nd Danubia-Adria Symposium on Experimental Methods in Solid Mechanics, Parma, Session-C Paper no 60.

Schuh CA, Packard CE, Lund AC (2006). Nanoindentation and contact-mode imaging at high temperatures. J. Mater. Res. 21(3):725.

Beake BD, J.F Smith JF (2002). High-temperature nanoindentation testing of fused silica and other materials. Philosophy Magazine A. 82(10): 2179.

Volinsky AA, Moody NR, Gerberich WW (2004). Nanoindentation of Au and Pt/Cu thin films at elevated temperatures. J. Mater. Res., 19(9):2650.

Sawant A, Tin S (2008). High temperature nanoindentation of a re-bearing single crystal Ni-base superalloy. Sci. Mater. 58(4):275.

Lu YC, Jones DC, Tandon GP, Putthanarat S, Schoeppner GA (2009). High temperature nanoindentation of PMR-15 polyimide. Exp. Mech. 50(4): 491.

Fulcher JT, Lu YC, Tandon GP, Foster DC (2010). Thermomechanical characterization of shape memory polymers using high temperature nanoindentation. Polymer Testing, 29(5):544.

Lu H, Huang G, Wang B, Mamedov A, Gupta S (2006). Characterization of the linear viscoelastic behavior of single-wall carbon nanotube/polyelectrolyte multilayer nanocomposite film using nanoindentation. Thin Solid Films, 500(1-2): 197.

Sneddon IN (1965). The relation between load and penetration in the axisymmetric boussinesq problem for a punch of arbitrary profile. Int. J. Eng. Sci. 3(1):47.

Lee EH, Radok JRM (1960). The contact problem for viscoelastic bodies. J. Appl. Mech.-T. ASME. 27:438.

Amatani T, Nakanishi K, Hirao K, Kodaira T (2005). Monolithic periodic mesoporous silica with well-defined macropores. Chem. Mater., 17(8):2114.

Sadr A, Shimada Y, Lu H, Tagami J (2009). The viscoelastic behavior of dental adhesives: A nanoindentation study. Dental Mater., 25(1):13.